CHAPTER IV
RESULTS AND DISCUSSION

In this Chapter, the results and discussion are classified into three parts. First, synthesis of the NaY zeolite by using different parameters is discussed in Section 4.1. In addition, changing the form of zeolite from ammonium to proton form is discussed in Section 4.2. Lastly, the catalytic activity of the prepared HY with different crystal sizes isdetermined in Section 4.3.

4.1 Synthesis of NaY Zeolite

NaY zeolite was synthesized by using sodium aluminateas an alumina source and colloidal silica as a silica source. The desired molar ratio composition of sodium aluminosilicategel obtained from experiment is$4Na_2O$: $1Al_2O$: $10SiO_2$: $180H_2O$.

The gel solution was aged at room temperature for 24 h under high agitation conditionsand then treated at 100°C for 2 h. After the crystallization process by using microwavedigestion, the white solid wasobtained and identified by various characterization techniques including XRD, XRF, BET and SEM methods. Figure 4.1 shows the XRD pattern of prepared NaYzeolite. The XRD resultsshowed the normal diffraction pattern of synthesized zeolite NaY(2θ = 6.17, 10.12, 11.87, 15.62, 18.67, 20.31, 22.78, 23.58,24.92, 25.73, 26.99, 27.68, 29.55, 30.81, 31.36, 32.41, 33.03, 34.06, 34.61, 35.59 and 37.77). The physical and chemical properties of the synthesized NaYare shown in Table 4.1.

Table 4.1 Physical and chemical properties of the synthesized NaY zeolite

Zeolite	Surface area (m^2/g)	Crystal size (μm)	Na_2O (%)	SiO_2/Al_2O_3
NaY-T100A1	670.7	0.7	15.98	3.64

*T = Crystallization Temperature
A = Aging time

The BET surface area, pore volume, and pore size of the prepared NaY weredetermined. The results indicated that the value of total surface area was 670.7m^2g^{-1}.The crystallite size of the prepared NaY zeolite was observed by scanning electron microscope as shown in Figure 4.2. The average crystallite size of prepared NaY zeolite was 0.7 μm thatwas smaller sizes compared with the commercial HY zeolite. The ratio of SiO_2/Al_2O_3 of NaY zeolite determined by X-rayfluorescence was3.64.

The different amounts of Si and Al between the gel composition and final product could be explained that there is no quantitative correlation between the Si/Al in the product and in the batch composition even if the Si/Al ratio in the parent mixture plays an important role in determining the structure and composition of the final product. The Si/Al ratio in the precursor gel is always higher than that in the crystallized product and the excess of silicon is left in the mother liquid. Moreover, the faujasite type of zeolite could only be synthesized within a narrow SiO_2/Al_2O_3 ratio from a specified batch composition with a narrow Si/Al ratio in the range of 6-14 molar ratios (Ruren, X *et al.*, 2007).

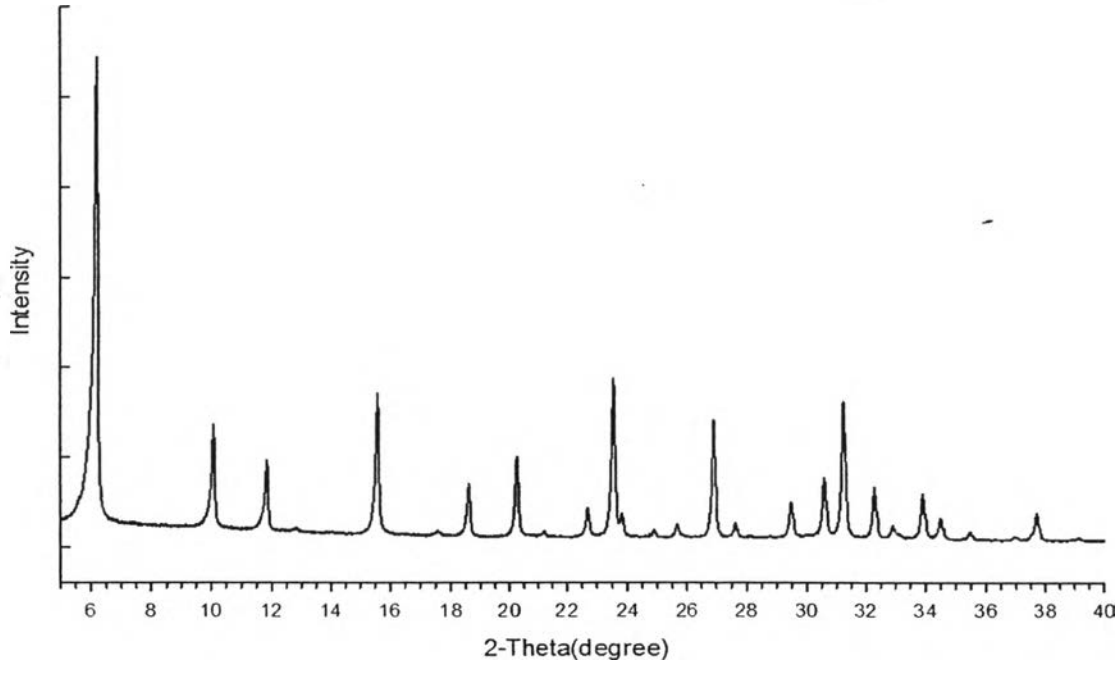

Figure 4.1 XRD pattern of synthesized NaY zeolite.

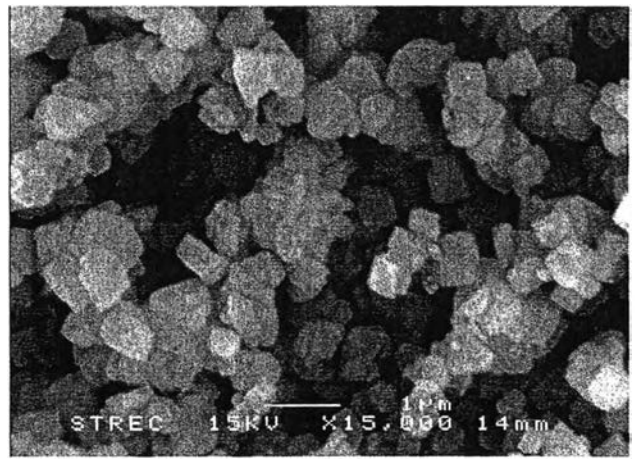

Figure 4.2SEM image of synthesized NaY zeolite.

The morphology of NaY zeolite obtained from microwave hydrothermal synthesis was depicted in Figure 4.2. It was found that synthesized NaY zeolite has a various type of morphology structures. The result could be explained by microwave radiation effect. Microwave irradiation was more efficient for transferring thermal energy to a volumeof alumino-silicate amorphous gel than conventional thermal processing whichtransfers heat to the material by convection, conduction. Therefore, the growth direction by using the microwave hydrothermal method was originally grown from the inside by the vibration of the molecules, thus resulted in fast and several way crystallization to form the different morphology.

4.1.1 Optimization of the Crystallization Time on Crystallinity

The properties of each prepared Y zeolites in sodium form were investigated by usingan X-ray diffractometer, with the aim of optimizing the crystallization time during the microwave hydrothermal synthesis process (M-H). Figure 4.3 shows XRD diffraction patterns of samples that were synthesized at 100°C for the different periods of time (0.5, 0.75, 1, 2, 3, 4, 5 h). The obtained XRD patterns showed a crystallizationphases and also thedegree of crystallinity of prepared NaY zeolite. The results showed thatprepared the NaY zeolite had a completedstructure after crystallization for2 h. After 2 h (3, 4, and 5 h), the prepared NaY had approximately the same

crystallinity. Moreover, it was seen tobe relatively similar to the XRD patterns of the referenceNa-Faujasitesample as shown in Appendix B.

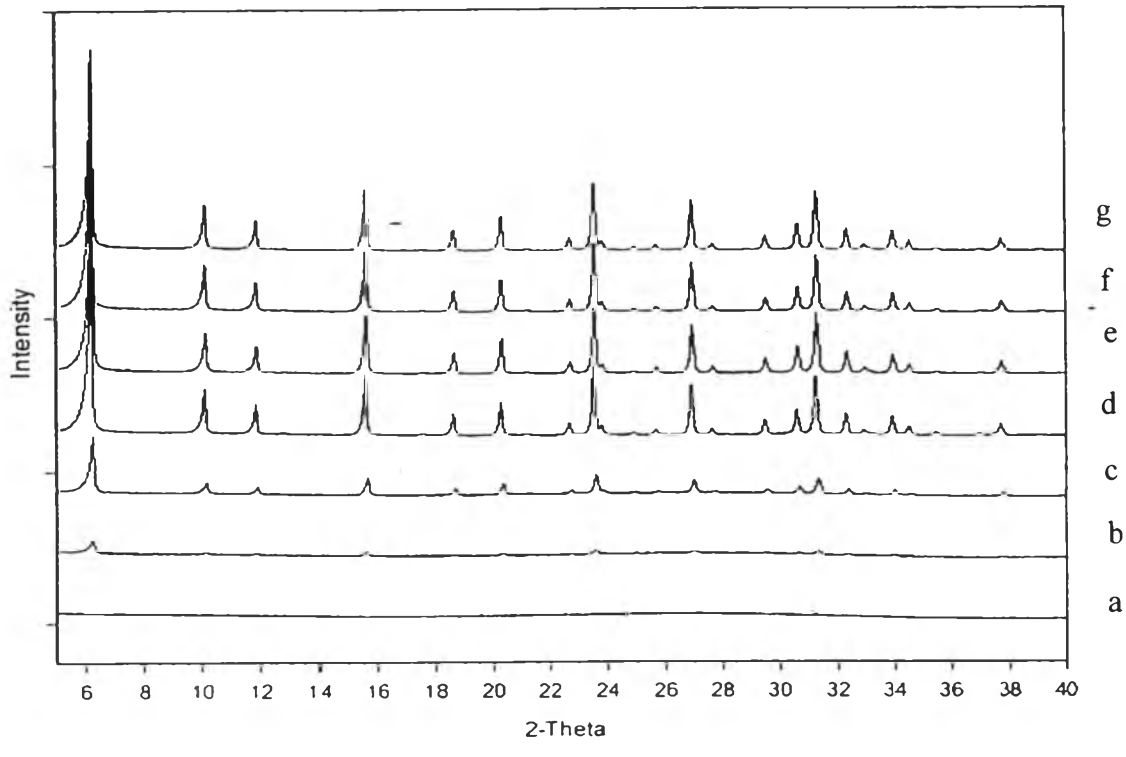

Figure 4.3 XRD pattern of synthesized zeolite NaY at different crystallization times(a) 0.5, (b) 0.75, (c) 1, (d) 2, (e) 3, (f) 4, (g) 5 h.

Thecrystallization time of 2 hwas the shorttest crystallization time thatcould provide an appropriate degree ofcrystalline zeolite. Therefore, the crystallization time of 2 h was selected as theoptimumtime for further study.

4.1.2 Effect of Crystallization Temperature on Crystallite Sizes of NaY Zeolite

In this study, the effect of crystallization temperatures in the range of90, 100, 110°Con the crystallite size and crystallinity was investigated. The average particle sizes of the zeolites prepared at different temperaturesare shown in Figure 4.4.

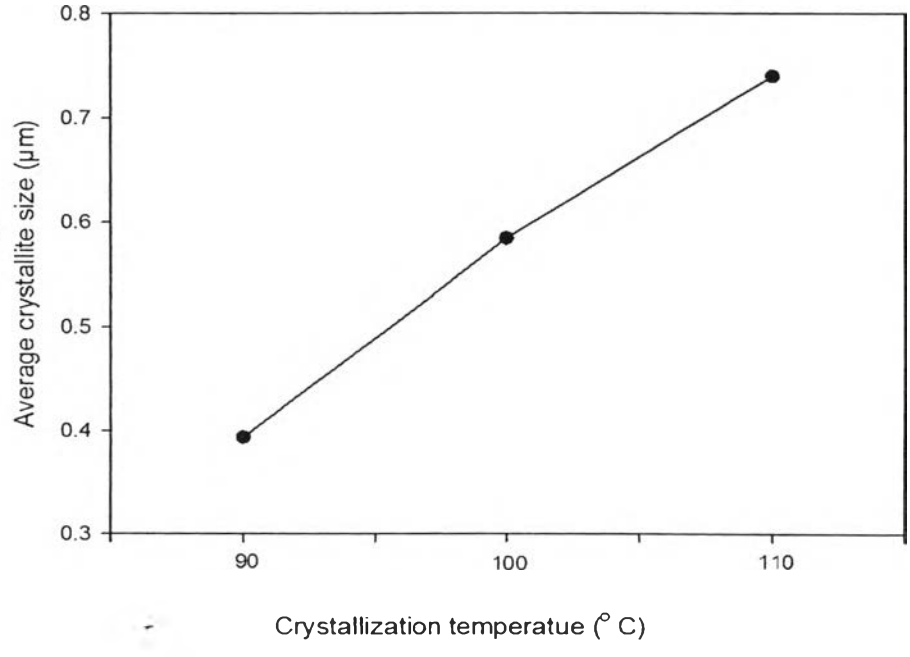

Figure 4.4 Crystallite size of the prepared NaY zeolite at different crystallization temperatures (90, 100, 110 °C).

Shape and average crystallite size of the NaY zeolite was alsoobserved from scanning electron microscopy (SEM) as shown in Figures 4.5 and the average crystallite size was calculated from

$$\text{Average crystallite size} = \frac{\Sigma\,[(\text{particle size was measured from SEM}) \times (N)]}{N}$$

Where N= number of crystal sample

The result showedthat 110°C gave a highest crystallite size. Decreasingcrystallization temperature gavea smaller zeolite crystal because higher temperature could accelerate the growth of crystal, resulting in larger crystals. The decreased

temperature was more favorable to the nucleation than crystal growth, resulting in smaller zeolite.

A similar result has been reported by Zhdanov *et al.* for the synthesis of NaA zeolite. Typically the particle size of zeolites depends on the relative rates of the two competing phenomena occurring during synthesis between nucleation and crystal growth. Both rates decreased with decreasing temperature, however, the impact was more pronounced on the crystal growth rate than on the nucleation rate resulting in smaller crystallite size at lower temperature.

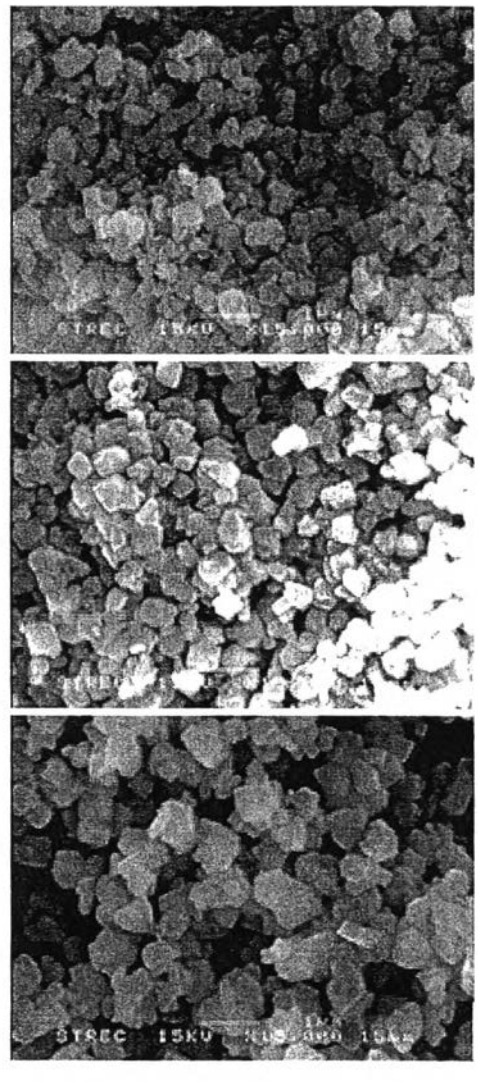

Figure 4.5 Scaning electron micrographs of prepared NaY zeolite atdifferent crystallization temperatures (a)90, (b) 100, (c) 110 °C.

However,Figure 4.5(a)showed that the prepared NaY sample exhibited some amorphous phase at the 90°C distinctly. These results were consistent with XRD results which is shown in Figure 4.6because thetoolow temperature in the crystallization step was favorable for the fast nucleation of NaY zeolite without crystal growth in crystallization step, some amorphous phase in the was occurred.

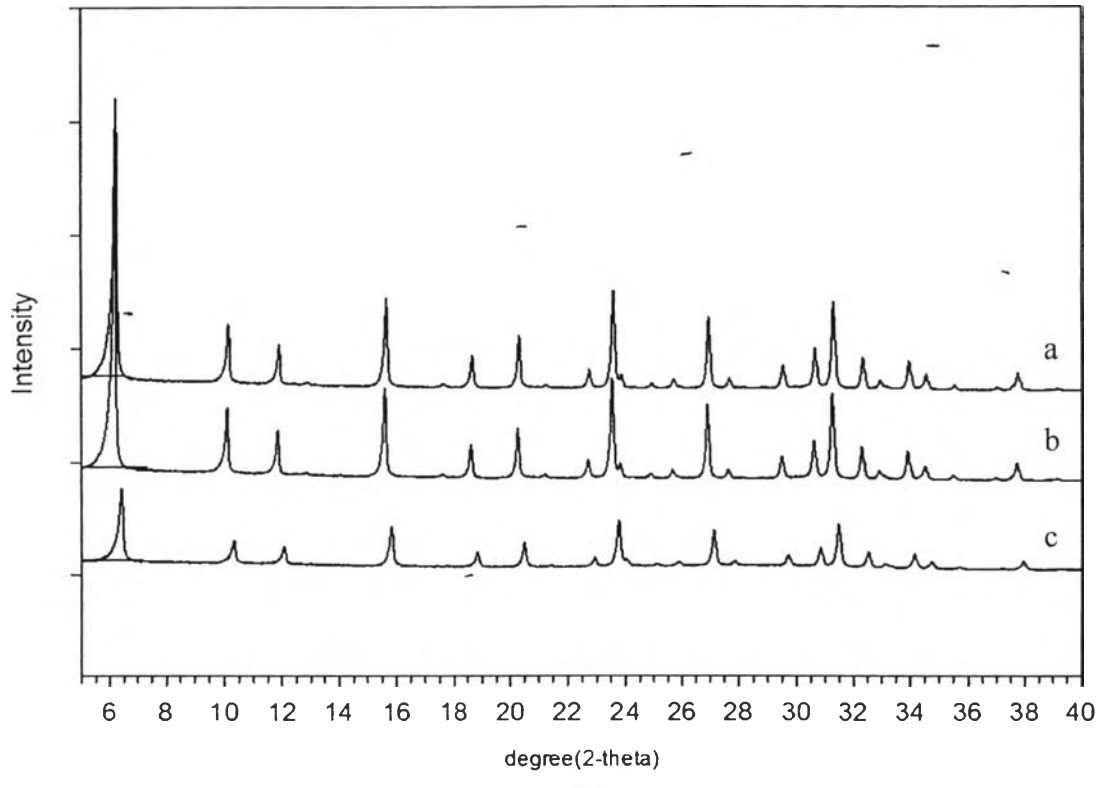

Figure 4.6 XRD pattern of synthesized zeolite NaY at different crystallization temperatures(a) 90, (b) 100, (c) 110 °C.

4.1.3 Effectof Aging Timeon Crystal Size of NaY Zeolite

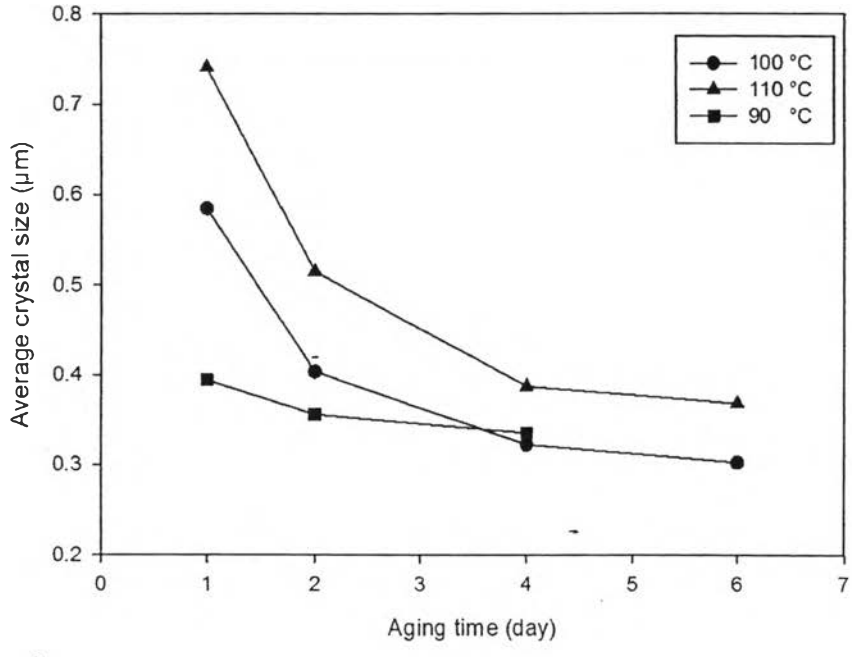

(a)

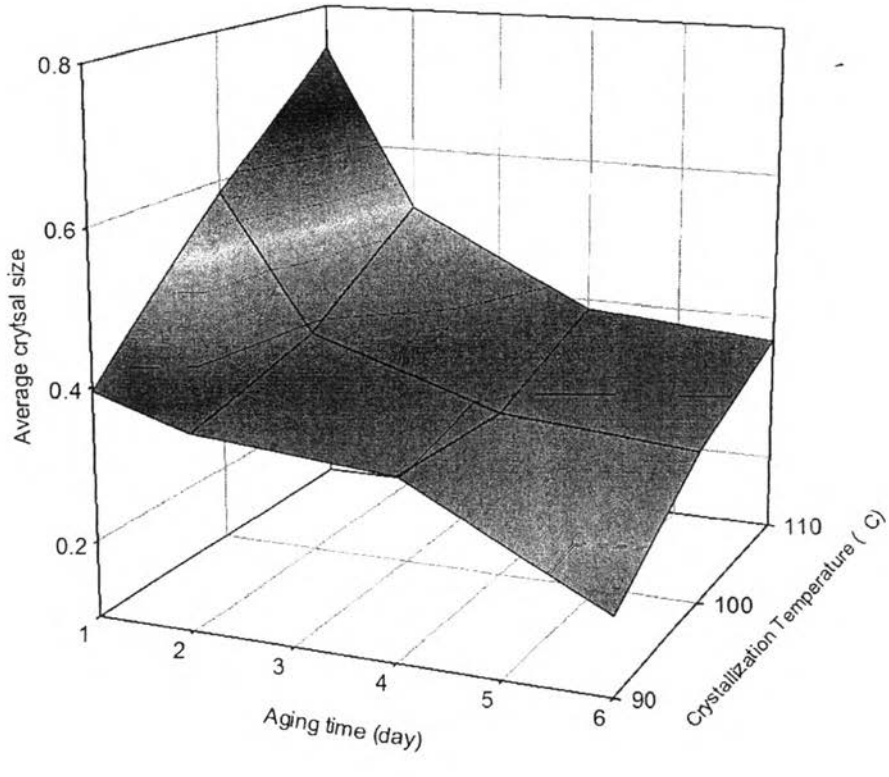

(b)

Figure 4.7 Crystalsize of the prepared NaY zeolite at different aging times(day). (a) Two-dimensional plot, (b) Three-dimensional plot.

The plot of average particle sizes of Y zeolite as a function of aging times(1, 2, 4and 6 days)are shown in Figure 4.7. At 100 °C, the results showed that the average crystallite size of the samples decreased from 0.6 to 0.4, 0.32, and 0.30 μm when the aging time increased from 1 to 2, 4 and 6 days,respectively. A similar trend was observed for all crystallization temperatures.

These resultsindicated that longer aging time of nucleation gave smaller crystals. As the longer aging time may allow an increase in the number of nuclei or nuclei precursors, the final average crystal size was decreased. Julide*et al.* reported that the aging the synthesis mixture prior to crystallization is a common method used to tailor the size of zeolite crystals.Especially at room temperature, they concluded that the nucleation rate was significant at room temperature while the growth rate was negligible.Nuclei precursor was growth until the temperature was increased.

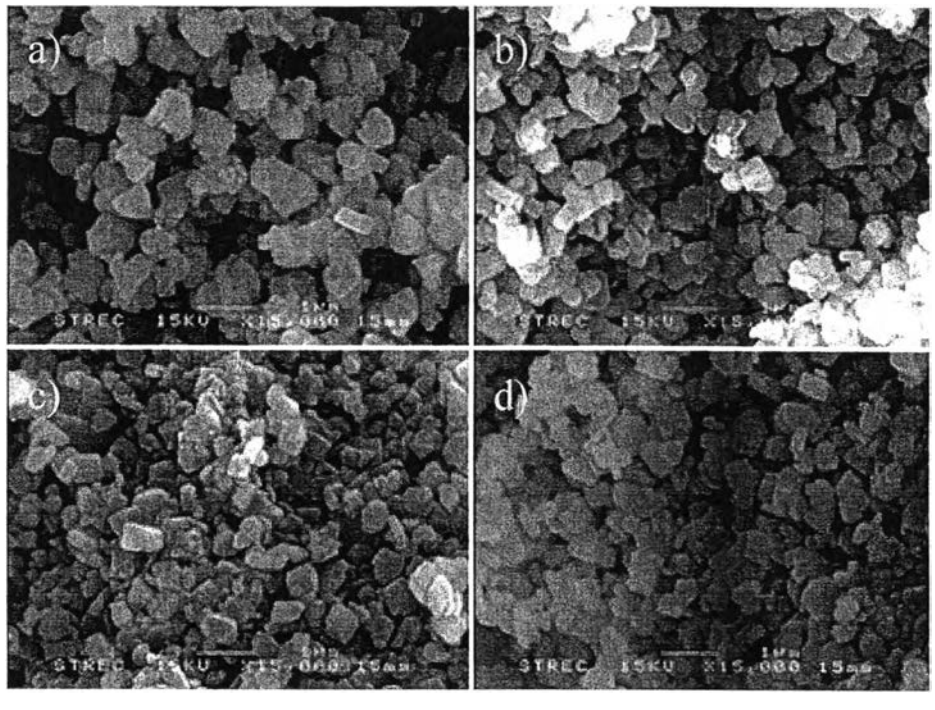

Figure 4.8 Scanning electron micrographs of prepared NaY zeolite indifferent aging times (a) 1, (b) 2, (c) 4, (d) 6 days at crystallization time 110 °C.

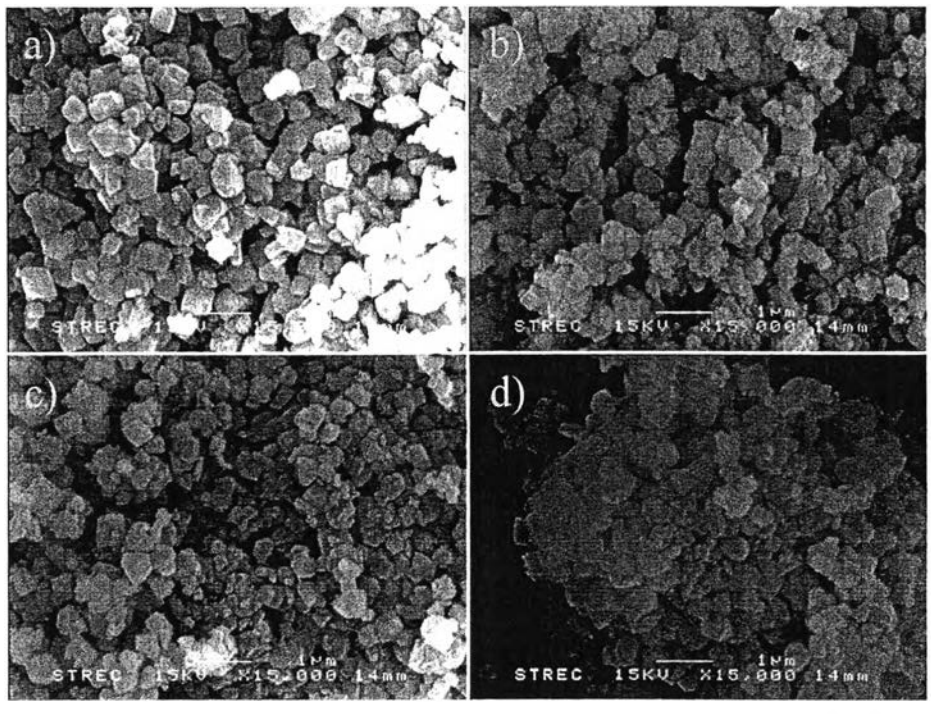

Figure 4.9 Scanning electron micrographs of prepared NaY zeolite indifferent aging times (a) 1, (b) 2, (c) 4, (d) 6 days at crystallization time 100 °C

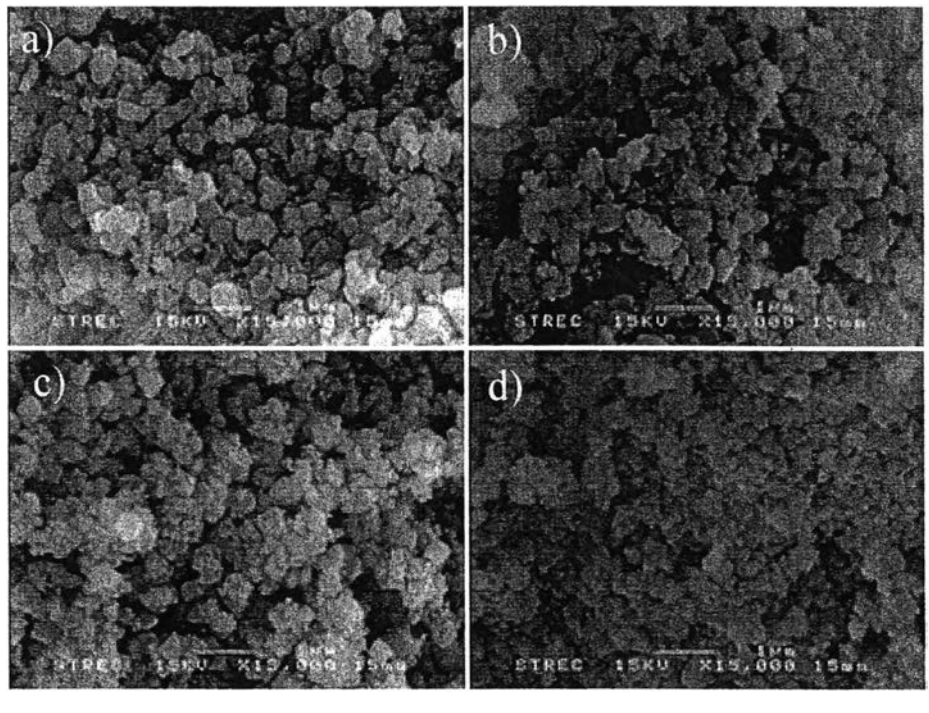

Figure 4.10 Scanning electron micrographs of prepared NaY zeolite indifferent aging times (a) 1, (b) 2, (c) 4, (d) 6 days at crystallization time 90 °C.

The morphologicalimages from scanning electron microscopy (SEM) of prepared NaY zeolite on different aging times areillustrated in Figures 4.8, 4.9, and 4.10. The results indicated that crystals with different shapes and sizes were formed. This observation is associated with the X-ray diffraction analysis results. However, in the aging time of 6 days that seem to be an agglomerated crystal due to the presence of much more nuclei in the system,it can be concluded that too long aging time in the synthesis process is a negative effect during the nuclei formation process.

4.1.4Effect of Alkalinity (Na_2O/Al_2O_3Molar Ratio)on Crystal Size of NaYZeolite

In order toinvestigate the effect of alkalinity on crystallite size of Y zeolite, a starting molar composition of xNa_2O: $1Al_2O_3$: $10SiO_2$: $180H_2O$ was chosen with different amounts of Na_2O, where x was varied from 4to 7 moleswith 24 h of aging time and crystallization temperature of 100 °C for 2 h.The average particle sizes of Y zeolite obtained from different Na_2O/Al_2O_3molar ratio are shown in Figure 4.11.

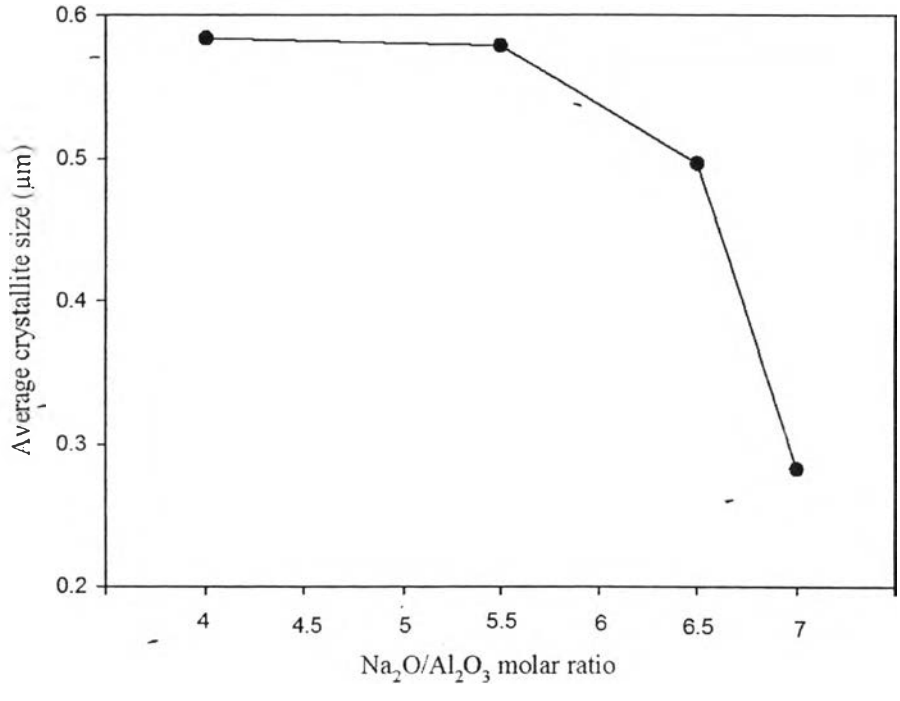

Figure 4.11 Crystallite size of the prepared NaY zeolite at different Na_2O/Al_2O_3 molar ratios.

The morphology images from scanning electron electroscopy (SEM) of prepared NaY zeolite on different Na_2O/Al_2O_3 molar ratio are demonstrated in Figures 4.12. The results obviously demonstrated that the higher Na_2O concentration gave a decreased crystallite size of Y zeolite because the higher Na_2O content would produce more nuclei,leading to smaller crystals. A similar result has been reported by Sathupunya*et al.*, (2002)for synthesis of NaA (LTA) with the sol-gel microwave me-

thod. The use of more Na_2O implies increased OH^- concentration (OH^-/Al_2O_3molar ratio=2(Na_2O/Al_2O_3 molar ratio)), then the increase in Na_2O concentration increased the hydroxyl concentration, which in turn enhanced the dissolving rate of amorphous gel of growing crystal that could improve nucleation rate step leading to the growth of more crystals, leading to smaller crystals.

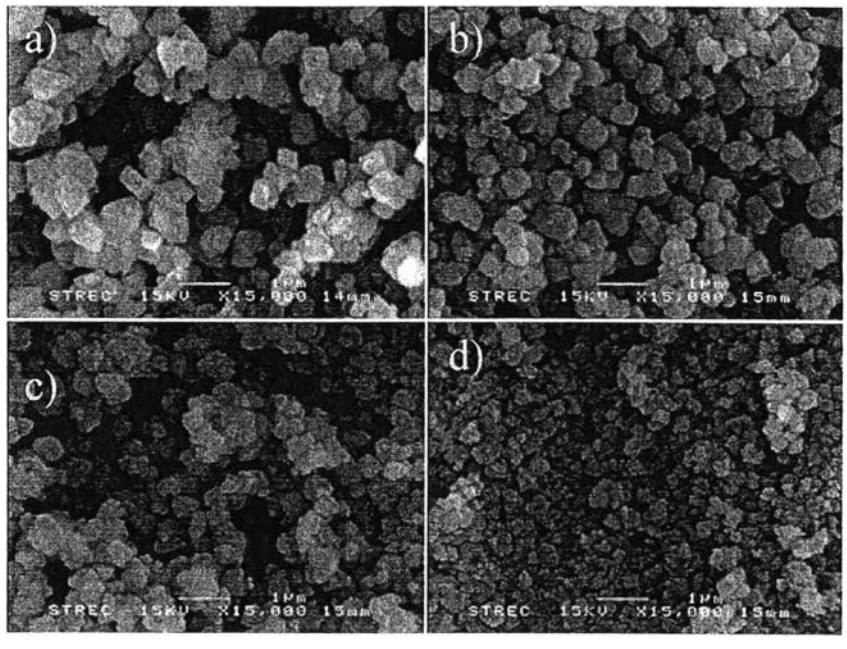

Figure 4.12 Scanning electron micrographs of prepared NaY zeolite indifferent Na_2O/Al_2O_3 molar ratios obtained from xNa_2O: $1Al_2O_3$: $10SiO_2$: $180H_2O$ molar ratio: (a) 4, (b) 5.5, (c) 6.5 and (d) 7 moles, respectively.

4.2 Preparation of HY Zeolite from NaY Zeolite

The ammonium form (NH_4Y) of Y zeolite wasobtained by substitution of the original sodium ions with ammonium nitrate (NH_4NO_3) and ammoniumhydroxide (NH_4OH) solution as the ammonium precursor. The ammonium exchanged zeolite was then calcined to obtain protonic form of Y zeolite (HY).

The structure of the Y zeolite after ammonium exchanged and calcinedwas also investigated using X-ray diffractometeras shown in Figure 4.13.

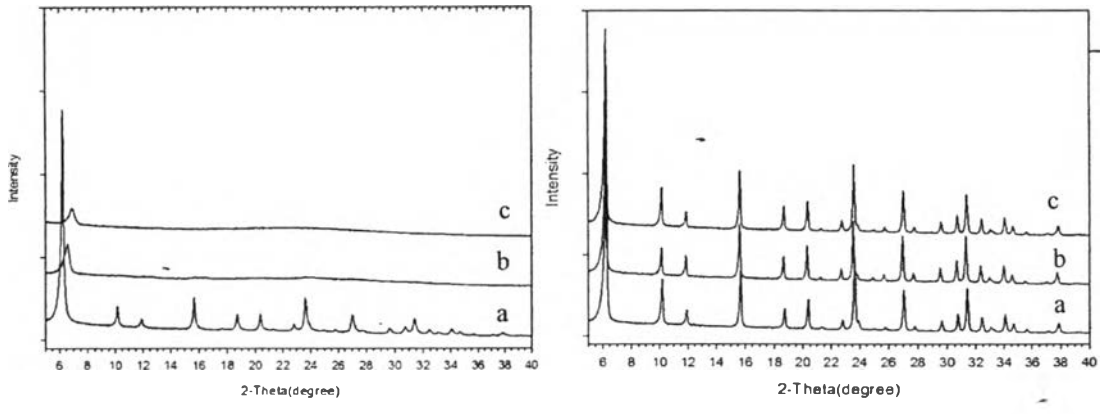

Figure 4.13 XRD pattern of HY with after ammonium nitate (left), ammonium hydroxide (right) exchanged: (a)1ststage,(b) 2nd stage, (c)3rd stage.

The results showed that the structures after exchanged with ammonium nitrate (NH_4NO_3) and ammonium hydroxide (NH_4OH) solution weresignificant different as depicted in Figure 4.13. The structure of HY zeolite after 3rd stage ion exchanged with the NH_4NO_3 was collapsed. However, in case of exchanged with the NH_4OH precursor, the structure was still remained.The results revealed that the NH_4NO_3 wasa violently exchangeable precursor.When it was exchanged with the prepared Y zeolite which a low strength and Si/Al ratio, the structure would be collapsed and loss of crystallinity.

The effect could beclearly explained by the mechanical properties of synthesized Y zeolite by using microwave digestion method. Although, microwave heating could remarkably reduce synthesis time and crystal sizes of Y zeolite, the

strength of small crystalsizes of Y zeolite wasless than the commercial Y zeolite.And the cumulative thickness of zeolite was reduced because the crystallization rate was greatly accelerated by microwave synthesize.Moreover, the prepared NaYzeolite hada Si/Al less than 5which had a lot of unstable point (O- Al bond) so the mechanical properties was not good (Yanshuo Li *et al.*, 2007).

Figure 4.13 (right) shows the XRD diffraction pattern of exchanged HYzeolite with NH_4OH in each stage. The results indicated that there were only a slight differencebetween the XRD pattern for NaY form and NH_4Y form. Although the main peaks of XRD patterns of the HY zeolite after three stages ion exchange did not change, the background decreased slightly. It could generally be suggested that the framework of zeolite was not widely affected, even though the sodium bonds were broken down inside its atomic structure.

Table 4.2 Relationship between the quantities of Na ion and acidity in number of exchanged treatment and type of ammonium precusor

Type of ammonium precursor	Number of Exchanged Treatment	Na^+ content (%wt)	Bronsted site (μmol/g)
NH_4OH	1	13.19	472.33
	2	11.45	680.23
	3	7.35	891.02
NH_4NO_3	1	10.72	-
	2	8.32	-
	3	0.22	-

The concentrationof Na^+ inside each sample was confirmed by using X-ray fluorescence (XRF) technique, which indicated that after the exchanged three times with NH_4OH and NH_4NO_3 precursor, the percentage ofNa^+ content within the framework of exchanged zeolite was decreased from 15.9 wt% to 7.35 and 0.22wt%,respectively as shown in Table 4.2. The results in these two different am-

monium precursor indicated that the ion-exchanged efficiency of the ammonium nitrate wasdramatically higher than the ammonium hydroxide because the enthalpy formation of ammonium hydroxide was exothermic. When the temperature increased, the reaction would be reversible also.The formation of ammonium hydroxide could be expressed by the following Equation 4.1.

$$NH_{3\,(aq)} + H_2O_{(l)} \longleftrightarrow NH_4^+{}_{(aq)} + OH^-_{(aq)} + 80.8\ KJ/mol \quad (4.1)$$

The reversible arrows showed that the reaction did not go to completion.Sometimes, only about 1% of the ammonia had actually reacted to form ammonium ions.

The influence of dissociation of this precursor could explain the lower exchange capacity which observed from prepared HY zeolite in this research.It probably resulted from a bad accessibility diffusion of the cationic positions (NH_4^+) into the Na ions surface of the NaY zeolite.

Furthermore, the value of acidity of the prepared HY zeolite was calculated based on the results obtained from thetemperature programmed desorption (TPD) of isopropylamine that catalyzed the conversion of the isopropylamine into propylene and ammonia (Pereira C., and Gorte R.J., 1992)as shown in Figure 4.14.The acidity of all exchanged catalystsis summarized in Table 4.2. It was found that the acidity of the catalysts increased with increasing exchanged step. The decreasing in acidity due to the exchanging of NH_4^+ with the Na^+ on the zeolite and the decomposing the NH_4^+cations by the calcination at 500 °C.The decationization of the zeolite and the thermal decomposition of the ammonium ion could be expressed by the following Equations 4.2 and 4.3.

$$NaY_{(s)} + NH4^+{}_{(aq)} \longleftrightarrow Na^+_{(aq)} + NH4Y_{(s)} \quad (4.2)$$

$$NH_4Y_{(s)} \xrightarrow{\Delta} NH_{3\,(g)} + HY_{(s)} \quad (4.3)$$

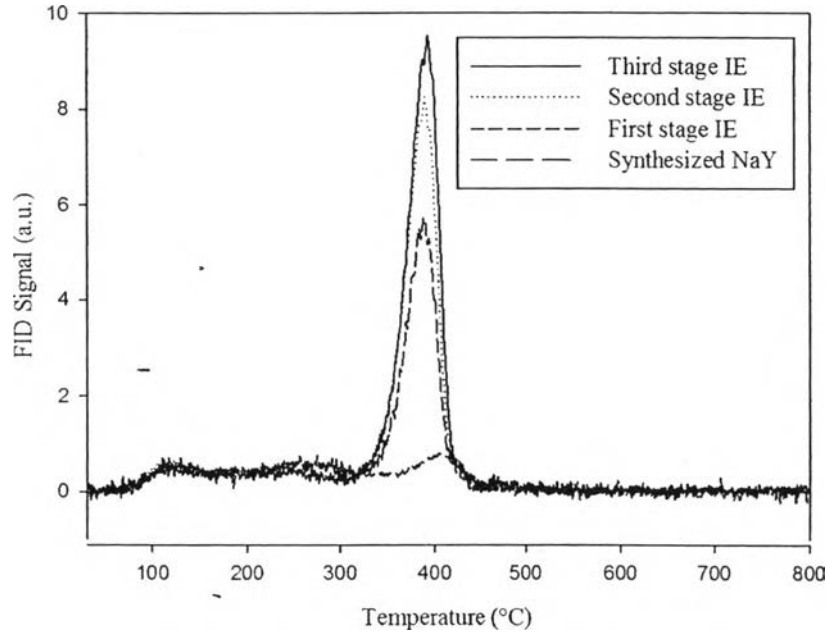

Figure 4.14TPD ofisopropylamine (IPA) of HY with different stage of ion exchanged with NH_4OH: m/z = 41, propylene/isopropylene.

4.3 Activity Testing

4.3.1Feed and Standard Analysis

The chromatogram and composition of hydrogenated biodiesel derived from jatropha oil (jatropha oil BHD) analyzed by a GC/FID (Agilent GC 7890) are shown in Figure 4.15 and Table 4.3, respectively. There are four main peaks representing *n*-pentadecane (C15), *n*-hexadecane (C16), *n*-heptadecane (C17) and*n*-octadecane (C18) that the retention times are at 25.54, 28.13, 30.52 and 33.72 min, respectively. Beside the *n*-paraffins, little amount of *iso*-paraffins was also observed. The first peak is carbon disulfide appeared at 1.23 and 1.39 min used as the diluent.

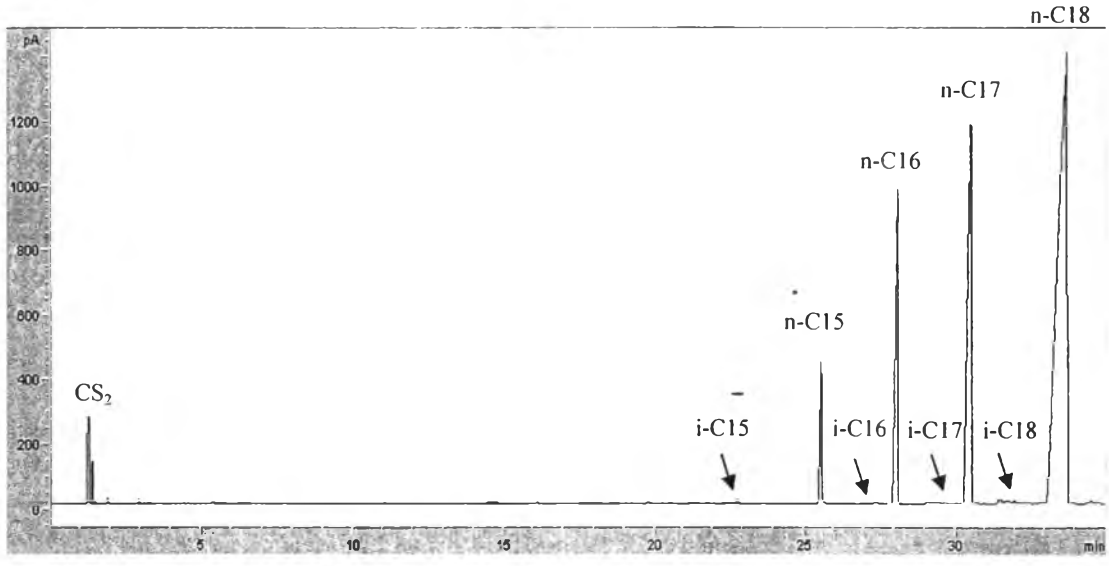

Figure 4.15 Chromatogram of hydrogenated biodiesel derived from jatropha oil analyzed by a GC/FID.

Table 4.3 Composition of hydrogenated biodiesel derived from jatropha oil analyzed by a GC/FID

Feed components	Amount (wt. %)
iso-Pentadecane (iso-C15)	0.11
iso-Hexadecane (iso-C16)	0.09
iso-Heptadecane (iso-C17)	0.27
iso-Octadecane (iso-C18)	0.94
n-Pentadecane (n-C15)	4.38
n-Hexadecane (n-C16)	14.25
n-Heptadecane (n-C17)	23.69
n-Octadecane (n-C18)	56.28

In order to identify the liquid product, it is necessary to know the retention times for each product peak by using mixture of standard chemicals. The FID signal of standard chemicals is shown in Figure 4.16 and the retention times for each standard chemical is listed in Table 4.4.

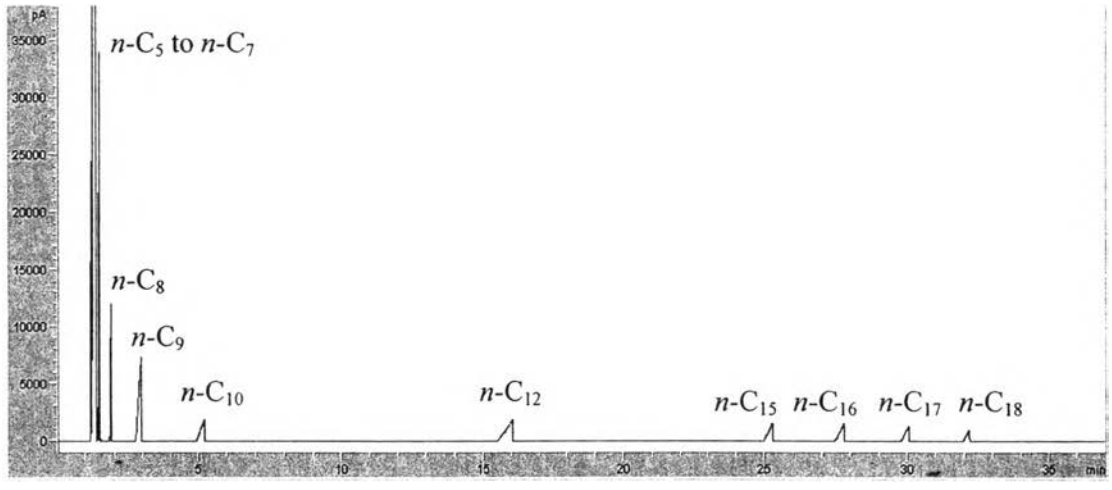

Figure 4.16 Chromatograms of standard chemicals including *n*-pentane (*n*-C_5), *n*-hexane (*n*-C_6), *n*-heptane (*n*-C_7), *n*-octane (*n*-C_8), *n*-nonane (*n*-C_9), *n*-decane (*n*-C_{10}), *n*-dodecane (*n*-C_{12}), *n*-pentadecane (*n*-C_{15}), *n*-hexadecane (*n*-C_{16}), *n*-heptadecane (*n*-C_{17}), *n*-octadecane (*n*-C_{18}) analyzed by a GC/FID.

For the reference standard of gas products, it was analyzed by a GC/FID (Shimadzu GC-17A) equipped with HP-Plot Al_2O_3 column. The FID signal of standard gas mixture is shown in Figure 4.17 and the retention times for each standard gas mixture are listed in Table 4.4.

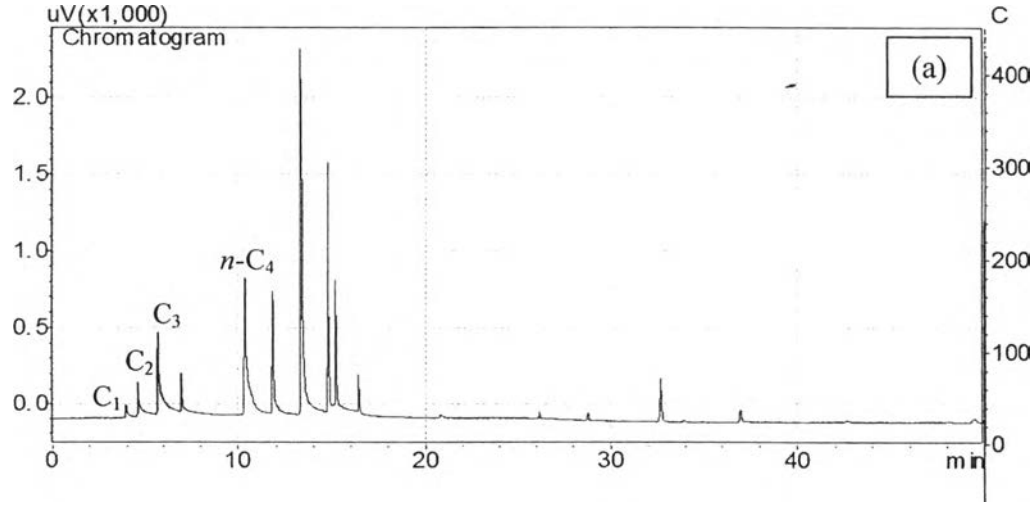

Figure 4.17 Chromatogram of the standard gases, (a) methane, ethane, propane and butane, (b) pentane, hexane, heptane, octane and nonane.

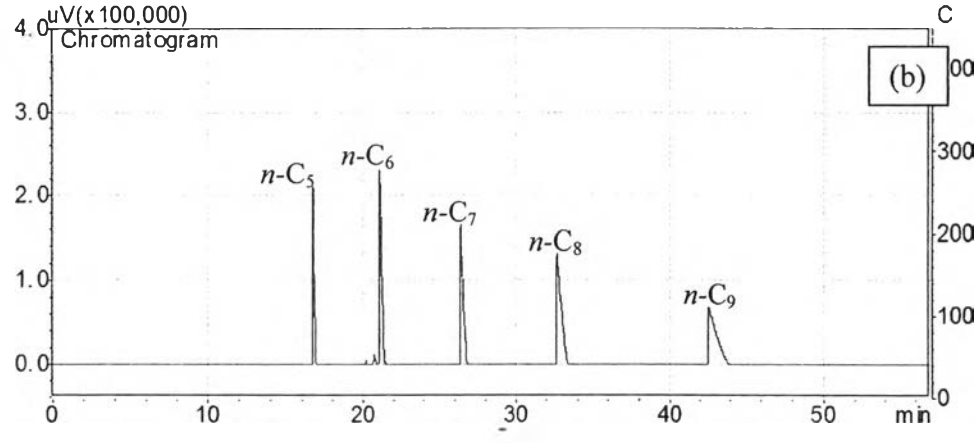

Figure 4.17(cont.) Chromatogram of the standard gases, (a) methane, ethane, propane and butane, (b) pentane, hexane, heptane, octane and nonane.

Table 4.4 Retention times of standard chemicals and standard gas mixture analyzed by a GC/FID (Agilent GC 7890A and Shimadzu GC-17A, respectively)

Standard chemicals	**Retention times (min)**	**Standard gas mixture**	**Retention times (min)**
n-Pentane (*n*-C_5)	1.14	Methane (C_1)	3.92
n-Hexane (*n*-C_6)	1.26	Ethane (C_2)	4.56
n-Heptane (*n*-C_7)	1.44	Propane (C_3)	6.96
n-Octane (*n*-C_8)	1.89	*n*-Butane (*n*-C_4)	11.80
n-Nonane(*n*-C_9)	2.95	*n*-Pentane (*n*-C_5)	15.95
n-Decane (*n*-C_{10})	5.46	*n*-Hexane (*n*-C_6)	20.32
n-Undecane (*n*-C_{11})	11.19	*n*-Heptane (*n*-C_7)	26.13
n-Dodecane (*n*-C_{12})	16.26	*n*-Octane (*n*-C_8)	32.30
n-Tridecane (*n*-C_{13})	19.97	*n*-Nonane (*n*-C_9)	41.73
n-Tetradecane (*n*-C_{14})	22.96		
n-Pentadecane (*n*-C_{15})	25.95		
n-Hexadecane (*n*-C_{16})	28.39		
n-Heptadecane (*n*-C_{17})	30.76		
n-Octadecane (*n*-C_{18})	33.52		

For example, chromatograms of liquid and gas products obtained over Pt/HY (Si/Al ratio of 3.8) operated at operating conditions: 450°C, 500 psig, LHSV of 1.0 h^{-1}, H_2/feed molar ratio of 30, and TOS of 6 h are shown in Figure 4.18(a) and (b), respectively. In Figure 4.18 (a),the chromatogram of liquid products, can bedivided into three main parts which are gasoline fuel (C_5-C_9), jet fuel (C_{10}-C_{14}), and remaining feed or diesel fuel (C_{15}-C_{18}) at the retention times of 1.14-2.95 min, 5.46-22.96 min, and 25.95-33.52 min, respectively. Figure 4.18 (b) illustrates a chromatogram of gas products, consisting of light fuel (C_1-C_4) and gasoline fuel (C_5-C_8) at the retention times of 3.92-11.80 min and 15.95-32.30, respectively.

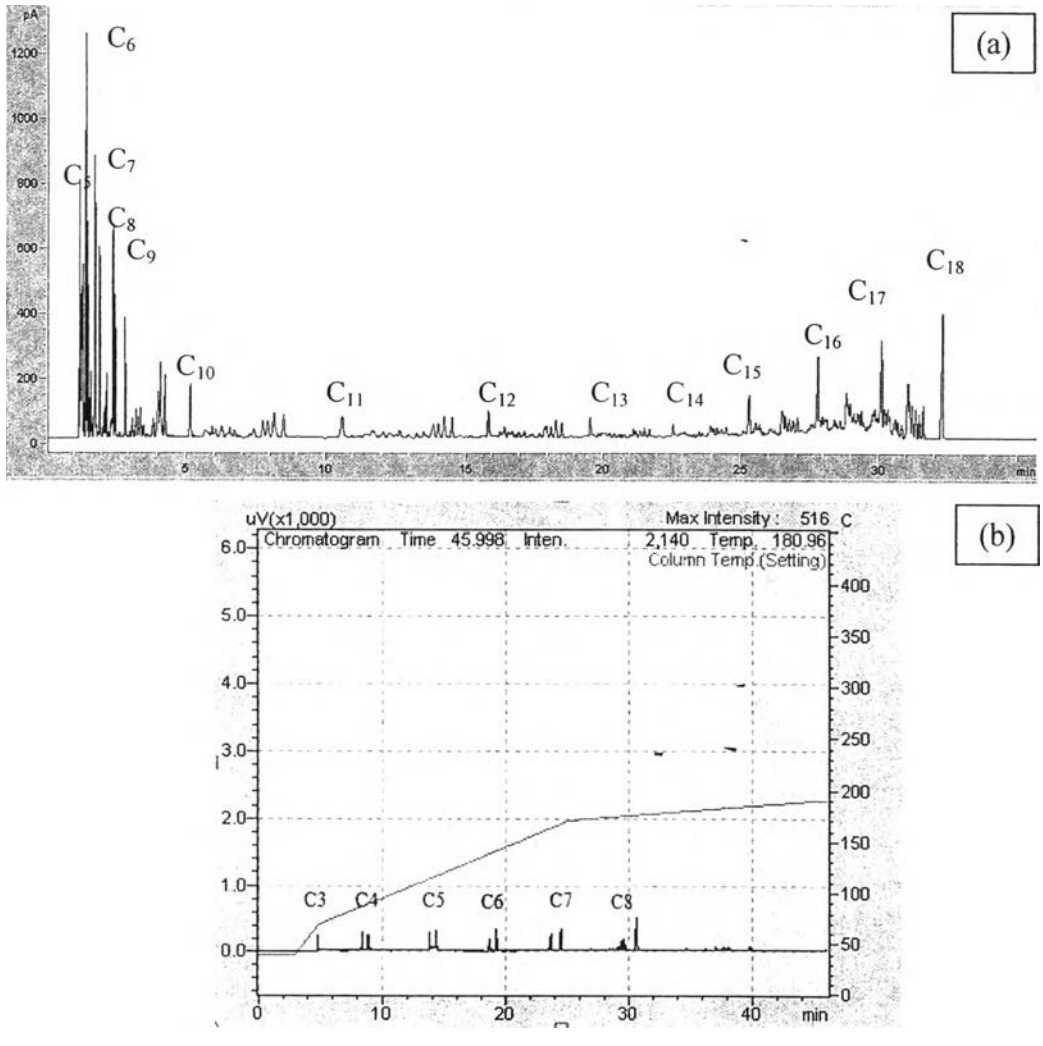

Figure 4.18 Typical chromatogram of (a) liquid products and (b) gas products over Pt/HY (Si/Al ratio of 3.8) operated at operating conditions: 450°C, 500 psig, LHSV of 1.0 h^{-1}, H_2/feed molar ratio of 30, and TOS of 2 h.

4.3.2Effect of Reaction Temperatures on Hydrogenated Diesel Cracking

The hydrogenated biodiesel conversion and product distribution obtained at 500 psig, liquid hourly space velocity (LHSV) of 1 h^{-1}, and H_2/feed molar ratio of 30 with different reaction temperatures are shown in Figure 4.19, the reaction temperature were varied from 350 to 450 °C. It could be seen that the yield of light, gasoline, jet increased with increasing cracking temperatures. The increase in yield related to the increase in a catalyst activity and reaction rate. According to the Arrhenius equation: $k = k_0 e^{-E/RT}$, with k is a reaction constant, k_0 is activity factor, E is activation energy, R is ideal gas constant and T is reaction temperature, k would be increased by increasing the reaction temperature. If k increased then the reaction rate was greater, so that the yield was also greater.

The maximum of the desired product was obtained at 450 °C. Therefore, the reaction temperature of 450 °C was selected as the optimum temperature for further study the effect of zeolite crystallite size.

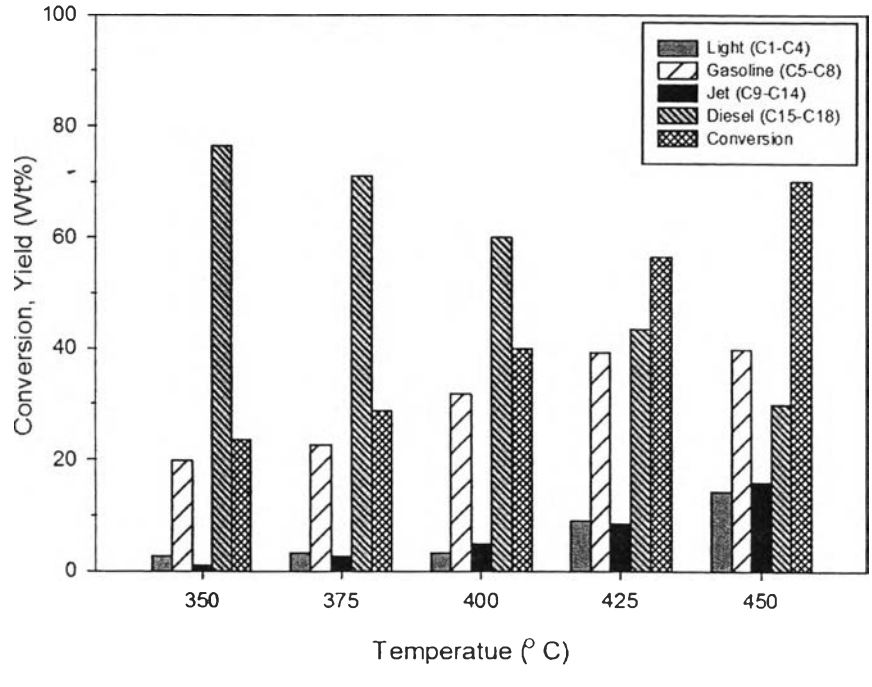

Figure 4.19 Yield of each product obtained over different reaction temperature of 0.3Pt/HY zeolite (Reaction condition:, 500 psig, LHSV of 1 h^{-1}, H_2/feed molar ratio of 30).

In this research, the increasing in reaction temperature could be explained by the local geometric and electronic structure of the bronsted site effect, which is influenced by the different form of zeolite (remaining of Na content in structure). The different electronic structure affected to the variation in the activation energies (E_a), which decreased in the opposite order: NaY> HY zeolite form. And according to $k = k_0 e^{-Ea/RT}$ equation, if E_a increased then the reaction temperature was increased, so that the reaction rate constant was also greater (Bin Xu *et al.*, 2006).

4.3.3Effect of Crystallite Size of Y Zeolite on Activity and Selectivity

For the catalytic activity and selectivity of the bi-functional catalysts, Pt supported HY catalysts with various crystallite sizes were investigated. The reaction conditions for hydrocracking of hydrogenated biodiesel were conducted at 450 °C, 500 psig, liquid hourly space velocity (LHSV) of 1 h^{-1}, and H_2/feedmolar ratio of 30.

Table4.5 BET surface area, external surface area, and pore volume of the synthesized Y zeolite with different crystallite sizes.

Sample	Particle size (μm)	BET surface area (m^2/g)	External surface area (m2/g)	Pore Volume (cm^3/g)
Y-T110A1	0.74	670.4	64.01	0.36
Y-T110A2	0.51	723.3	71.96	0.38
Y-T110A3	0.32	750.1	77.83	0.41

*T = Crystallization temperature
A = Aging time

The textural properties of Y zeolite with the different crystal sizes were obtained from the nitrogen adsorption isotherms using BET method are given in Table 4.5. The total surface areas of the different crystal size can be observed by comparing the corresponding surface area. The results showed that the differences in crystallite size affected in the values of surface area, the smaller crystallite size of Y zeolite gave a higher surface area and pore volume.

Figure4.20 illustrates the comparison of products defined as light range (C1-C4), gasoline range (C5-C8), jet range (C9-C14), and conversion of hydrogenated in different crystallite sizes. To investigate the catalytic performance of hydrogenated biodiesel cracking on different crystallite size of Y zeolite, three crystal sizes (0.75, 0.51 and 0.32 μm) of Y zeolite were used in this study.

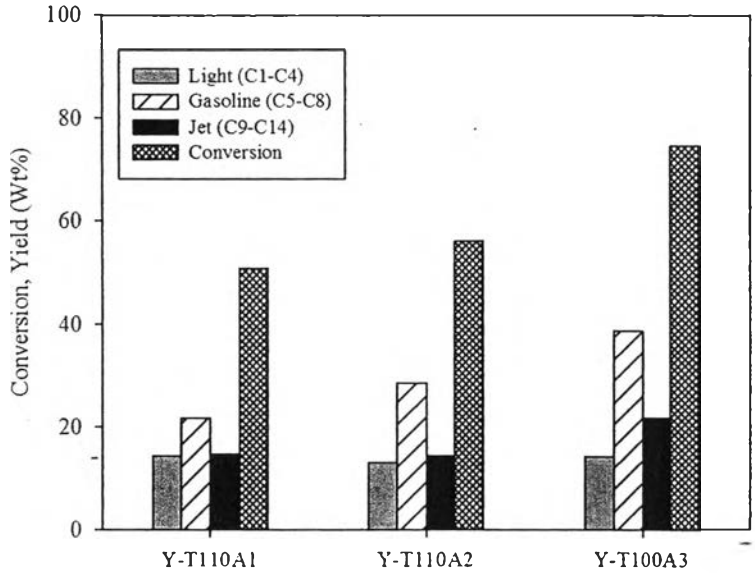

Figure 4.20 Conversion and yield obtained over different crystallite sizes of 0.3Pt/HY zeolite (Reaction condition: 450 °C, 500 psig, LHSV of 1 h^{-1}, H_2/feed molar ratio of 30 and TOS of 2 h).

The results showed that the smallest crystal size Y zeolite (0.32 μm)gave the highest conversion,which showed the highest yield of each product, followed by the 0.51 (Y-T110A2) and 0.74μm (Y-T110A1),respectively. These results indicated that the crystal sizes of zeoliteaffected in the catalytic activity, the smaller crystallite size exhibited higher catalytic activitydue to the improvement in the diffusivity of reactants and products. Moreover, the change of activity was attributed to the larger externalsurface area, leading to the following higher accessibility for large hydrocarbonmolecules. These results were in accordance with previous study of catalytic cracking of gasoil by using thesmall Y zeolite crystallites(M.A. Camblor. *et al.*, 1989). They reported that the result revealed a good correlation between the crystal size of zeolite and the activity: smaller naozeolite-based FCC catlyst gave higher catalytic activity.

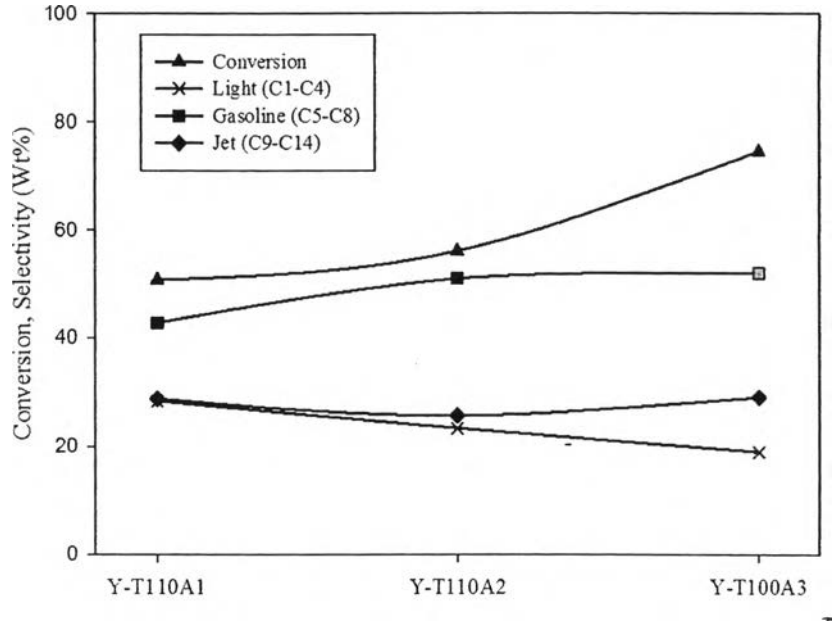

Figure 4.21 Conversion and product selectivity obtained over different crystallite size of 0.3Pt/HY zeolite (Reaction condition: 450 °C, 500 psig, LHSV of 1 h^{-1}, H_2/feed molar ratio of 30 and TOS of 2 h).

Figure 4.21shows the product ditribution and hydrogenated diesel conversion obtained over 0.3 Pt/HY zeolite at different crystallite sizes. The results showed that the conversion of hydrogenated biodiesel dramaticallyincreased with the crystal size decreased, the maximum of the conversion and desired product was obtained at crystallite sizes of 0.3 μm. for the product distribution, it has been found that amount of light yield significantly decreased with the smaller crystallite size. On the other hand, the higher amount of gasoline yield was obtained when crystallite size decreased. Then if we compared the jet selecticity of the different crystallite size, we found that sample Y-T110A2 (0.5μm) gave a slightly decreased of jet yield compared with the sample T110A1. However, T100A3 which has a 0.3 μm of crystallite size gave apparently higher jet selectivity.

The benefit of small crystallite size can contribute to a high selectivity of jet fuel and gasoline with low selectivity to light product. This result could be explained by the improved diffusion of reactants and products;accessibility of the

reactant in nanocrystalline zeolites enhanced the cracking activity as well as the desired product selectivity.

Table 4.6 Conversion, liquild, and gas products yield (Reaction condition: 450 °C, 500 psig, LHSV of 1 h^{-1}, H_2/ feed molar ratio of 30, and TOS of 2 h)

Catalysts		0.3Pt/HY		
		T110A1	T110A2	T100A3
conversion (wt. %)		50.75	56.04	74.54
Yield of gas Products (wt.%)	C1	0.77	0.94	3.29
	C2	3.73	3.92	3.30
	C3	5.64	6.85	4.83
	C4	4.26	1.38	2.74
	C5	6.93	6.45	13.86
	C6	2.87	5.82	1.16
	C7	3.98	4.12	4.10
	C8	0.99	4.32	4.97
Yield of liquid Product (wt.%)	iso-C5	0.11	0.23	0.33
	n-C5	0.47	0.72	1.35
	iso-C6	0.85	0.87	0.81
	n-C6	0.99	1.18	2.83
	iso-C7	0.99	1.08	1.43
	n-C7	1.13	1.22	3.61
	iso-C8	1.20	1.31	1.98
	n-C8	1.23	1.24	2.29
	iso-C9	1.55	1.64	2.36
	n-C9	1.24	1.20	2.02
	iso-C10	1.77	1.71	2.39
	n-C10	1.20	1.08	1.77
	iso-C11	1.69	1.49	2.20
	n-C11	1.00	0.95	1.45
	iso-C12	1.47	1.61	2.42
	n-C12	0.84	0.80	1.16
	iso-C13	1.34	1.41	2.28
	n-C13	0.75	0.66	0.89
	iso-C14	1.01	1.06	1.69
	n-C14	0.77	0.77	1.03
	iso-C15	1.97	1.79	2.06
	n-C15	1.85	1.70	1.16
	iso-C16	5.10	4.01	3.38
	n-C16	5.92	3.91	1.92

Table 4.6 (Cont.) Conversion, liquild, and gas products yield (Reaction condition: 450 °C, 500 psig, LHSV of 1 h^{-1}, H_2/ feed molar ratio of 30, and TOS of 2 h)

Catalyst		0.3Pt/HY		
		T110A1	T110A2	T100A3
Yield of liquid Product (wt.%)	iso-C17	7.30	6.08	5.28
	n-C17	5.50	5.40	2.25
	iso-C18	10.14	9.98	5.75
	n-C18	11.47	11.08	3.65
Yield of light (%)		14.40	13.09	14.16
Yield of Gasoline (%)		24.51	31.41	43.10
Yield of Jet (%)		11.84	11.54	17.28
Yield of Diesel (%)		49.25	43.96	25.46
Sum of iso-paraffins (wt.%)		36.48	34.30	34.39
Sum of n-paraffins (wt.%)		63.52	65.70	65.61

4.3.4Effect of LHSV

The effect of LHSV (reciprocal of contact time) on conversion and product distribution of hydrogenated biodiesel at constant reaction temperature of 450 °C and H_2/feed molar ratio of 30 are represented in Figures 4.22 and 4.23, respectively. The results showed that the hydrogenated biodiesel conversion decreased with the increasing of LHSV. The increased LHSV caused the decrease of product yields due to lower residence time.Moreover, the product selectivity as shown in Figure 4.23 exhibitedthat the jet selectivity decreased withincreasedcontact time, while the light selectivity increased. This effect can be explained that longer contact timecaused the secondary cracking in the zeolite pore, resulting in light and some gasoline.

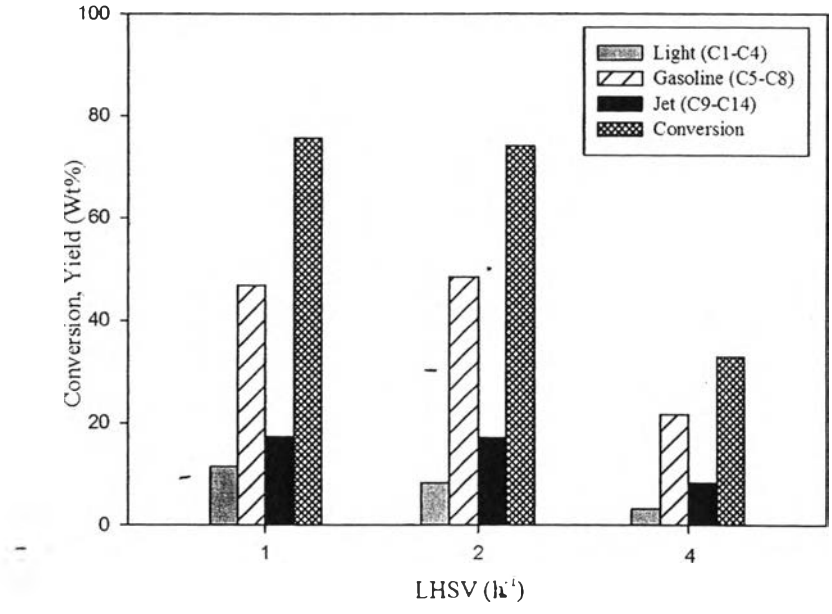

Figure 4.22 Yield of each product obtained over different liquid hourly space velocity (LHSV) of 0.3Pt/HY zeolite (Reaction condition: 450 °C, 500 psig, H_2/feed molar ratio of 30).

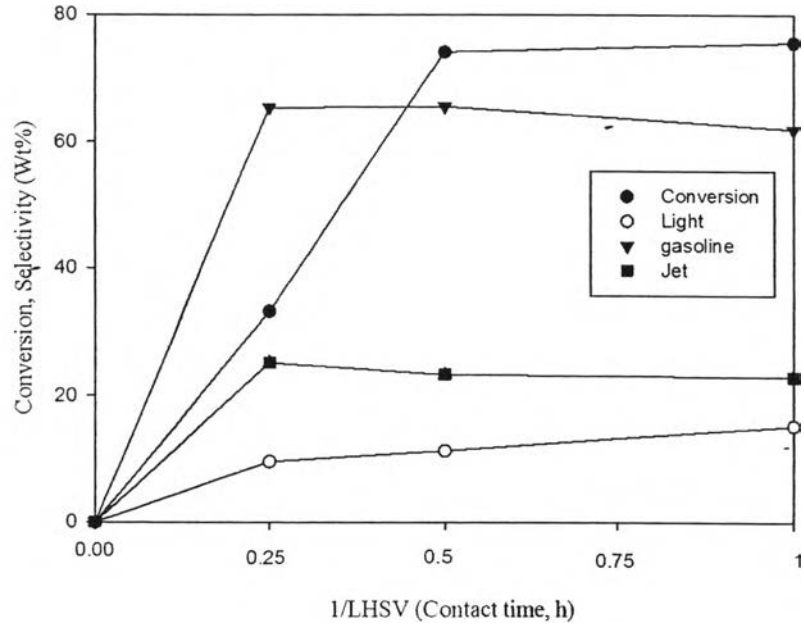

Figure 4.23 Product distribution (% selectivity) obtained over different liquid hourly space velocity (LHSV) of 0.3Pt/HY zeolite (Reaction condition: 450 °C, 500 psig, H_2/feed molar ratio of 30).

4.3.5Characterization of Spent Catalyst

The TPO profiles and amounts of coke deposit over spent catalysts (Y-T110A1, Y-T110A2, Y-T100A3) are illustrated in Figure 4.24 and Table 4.7, respectively. From all of spent catalysts sample, Y-T110A1exhibited the highest amount of coke deposit on the catalyst surface.

The results showed that the amount of coke formed after the reaction (TOS of 8 h) increased with decreasing crystal size due to the higher conversion in the small crystal size. Moreover the decrease in crystals size of Y zeolite affected the shifting of coke formation temperature; the smallest crystallite size gave the highest hard coke (high coke formation temperature). It is considered that the coke formation mainly occurred on the external surface of the zeolite crystals. As the smaller sized catalyst had more external surface area to accommodate the coke deposits and form the hard coke, the coke formation temperature was increased.

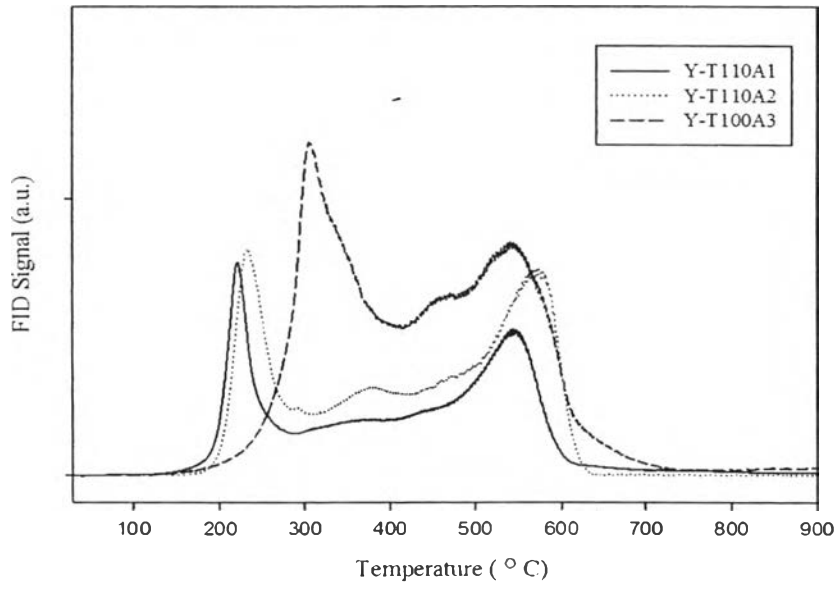

Figure 4.24TPO profiles of coke deposits left over the different crystallite size catalysts. Reaction conditions: temperature 450 °C, LHSV of 1 h^{-1} and H_2/feed ratio of 30.

Table 4.7 Amount of carbon deposit on 0.3Pt/HY catalyst after reaction with different crystallite size zeolite

Catalyst	Coke (wt. %)
Y-T110A1	4.78
Y-T110A2	6.78
Y-T110A3	7.86